Responses of channel morphology to flow-sediment variations after dam construction: a case study of the Shashi Reach, middle Yangtze River

Fan Chen, Li Chen, Wei Zhang, Jianqiao Han and Junzhou Wang

ABSTRACT

Upstream damming has profoundly impacted downstream channel morphology by altering inflowing water and sediment conditions, which can mostly be ascribed to variations in the flow hydrograph and sediment supply regime. In this paper, channel erosion and deposition during different flow-sediment processes are quantified using a 2D hydro-morphodynamic model. Our results revealed that the net erosion mainly occurred during the flood season when the flow discharges were above 15,000 m^3/s. Together, larger peak discharges and less sediment supply could produce greater net erosion. Flow hydrograph variations could alter the inundation extent, thus creating a more widespread redistribution of channel deposition and erosion and possibly causing a shift in the active channel adjustment area, where more channel scouring and siltation occurred. The channel adjustments caused by the sediment supply regime variations underwent a gradual downward propagation process, and most of the riverbed thalweg profile variations could first be observed at a very short distance from the studied reach entrance. A larger cross-sectional area and channel depth as well as a lower width-depth ratio could result from larger floods and less incoming upstream sediment load. We found that a comprehensive flow-sediment combination coefficient $(1/N)\sum_{i=1}^{N}(Q_i^m/S_i)/10^{4m}$ with a value of m ranging from 2 to 4 most appropriately reflected the post-dam flow-sediment imbalance regime at the studied reach, which implied the leading role of flow hydrograph variations in shaping channel morphology. In summary, the combined results presented herein for the Shashi Reach of the Yangtze River can provide a better understanding of the downstream morphological impacts of different flow-sediment processes caused by dam operation.

Key words | channel morphological adjustments, flow-sediment processes, sediment supply regime, Three Gorges Dam

Fan Chen
Li Chen (corresponding author)
Wei Zhang
Junzhou Wang
State Key Laboratory of Water Resources and Hydropower Engineering Science,
Wuhan University,
Wuhan, 430072,
China
E-mail: *chenliwuhee@whu.edu.cn*

Jianqiao Han
Institute of Soil and Water Conservation,
Northwest A&F University,
Yangling, Shanxi,
China

INTRODUCTION

The morphology of rivers is often the product of natural influences in combination with the effects of artificial projects (Biedenharn *et al.* 2000). In addition to natural events (Rădoane *et al.* 2013; Scorpio & Rosskopf 2016), human activities, such as gravel mining (Segura-Beltrán & Sanchis-Ibor 2013; David *et al.* 2016; Yuill *et al.* 2016), embankments, and hydropower schemes (Scorpio & Rosskopf 2016), can also heavily disrupt the normal patterns of flow and sediment transfer and even compromise the morphological and ecological functionality (Surian & Rinaldi 2003). Among these human activities, upstream damming is usually regarded as having the greatest anthropogenic impact (Tukur & Mubi 2002; Zahar *et al.* 2008; Pal 2016) and significantly changes the flow and sediment regime, thus altering the geomorphic processes and resulting in dramatic downstream channel adjustments (Xu 1996; Shields Jr

doi: 10.2166/nh.2019.066

et al. 2000; Topping et al. 2000; Yang et al. 2007; Smith et al. 2016).

As the largest dam in the world, the Three Gorges Dam (TGD) intercepts large amounts of sediment and modifies the seasonal distribution of flows (Chen et al. 2016; Wang et al. 2016), resulting in complex hydraulic and morphological responses downstream that have been elucidated from various perspectives. For example, Xu & Milliman (2009) examined the downstream sediment data from the TGD and indicated that the majority of sediment was trapped in the reservoir primarily during high-discharge months, which caused a decline in the rating curve and downstream channel degradation. Using *in situ* measurements and hydrological simulations, Wang et al. (2013) revealed an altered level regime in the middle and lower reaches of the Yangtze River as a combined result of flow regulation and sediment load reduction. Xia et al. (2016) calculated reach-scale bankfull channel dimensions based on an improved reach-averaged method and developed empirical relationships between the channel dimensions and corresponding incoming flow and sediment conditions. Notably, despite a variety of disturbances in the original equilibrium states of the fluvial system induced by the TGD, the altered flow and sediment fluxes are usually regarded as the two principle controlling factors that determine downstream channel morphological adjustments. The former is usually controlled by the natural runoff process and regulation strategy, while the latter is controlled by both the flow hydrograph and upstream sediment supply regime. Considering that the reduced flow discharge due to dam operation generally transfers less sediment and the cascade reservoirs at the upper Yangtze River will entrap more sediment, the sediment supplied to the downstream reach by the same flow discharge will be even less (Yang et al. 2014; Li et al. 2018a, 2018b).

The response of channel morphology to varying flow-sediment processes has attracted extensive attention and been investigated abundantly. Many studies have focused on the morphological significance of a single flow class, and due to the greater geomorphic impacts on channel reforming processes, the concepts of effective, bankfull, and channel-forming discharge have been widely used in the geomorphological impact analyses of floods (Lenzi et al. 2006; Surian et al. 2009; Ma et al. 2010; Shibata & Ito 2014). Other studies have attached great importance to the morphodynamic processes that occur during flashy floods or extreme floods (Guan et al. 2016; Rickenmann et al. 2016), and these studies have revealed the discrepancies between flow pulses and flood pulses (Bertoldi et al. 2010; Welber et al. 2012; Wyżga et al. 2016). In the abovementioned studies, a particular focus has been placed on the morphological significance of larger floods, and they suggested that the absence of less frequent floods may result in the narrowing of channels (Andrews 1986; Legleiter 2014), a reduction in the flooding extent (Graf 2006; Heitmuller 2014), and a decrease in the spatial scale on which morphological processes occur (Bertoldi et al. 2010). Although the morphological impacts of peak discharge reduction have been addressed repeatedly, the impacts of variations in upstream sediment load caused by different supply regimes have seldom been discussed and the channel morphological adjustments during different flow-sediment processes have mostly been investigated by field-observed data analyses, with few studies performing detailed comparisons via numerical simulations.

The 'real' post-dam fluvial process is collectively determined by both the regulated flow regimes and the gradually decreasing sediment supply. Previous studies have identified channel narrowing and deepening as well as an adjustment area transfer in reaches downstream of the dam (Graf 2006; Surian et al. 2009). However, these changes were frequently discussed as the final results of altered flow-sediment processes (Legleiter 2014; Scorpio & Rosskopf 2016; Smith et al. 2016; Zhou et al. 2017), and few changes were specifically related to the flow hydrograph or sediment supply variations, thus increasing the difficulty of discerning the roles of flow and sediment variations in affecting downstream river morphology. Hence, a special emphasis should be placed on the important discrepancies between these two factors, and a dam's downstream impacts should be investigated based on morphological adjustment sensitivities to different flow-sediment processes.

Therefore, the main objective of this work is to investigate the effect of different flow-sediment processes on the channel morphological adjustments downstream of the TGD using a 2D morphodynamic model. The research questions posed in this paper are as follows:

(1) How is the channel morphology of the studied reach changed during a post-dam hydrological year?

(2) How is the channel morphology changed during different flow-sediment processes?
(3) What influences do different flow hydrographs and sediment supply regimes have on the channel morphology?

STUDY AREA

The Yangtze River has a basin area of 1,800 thousand km^2 and a total length of 6,397 km, and it is usually divided into the upper, middle, and lower reaches according to different regional environments and hydrological conditions (Figure 1(a)). In the outlet of the upper Yangtze River lies the TGD, which is the largest hydroelectric power plant in the world and the most important water control project on the Yangtze River. About 102 km downstream of the TGD, the segment between Zhicheng and Chenglingji is known as the Jingjiang Reach, which can be further divided into the Upper Jingjiang Reach (UJR) and Lower Jingjiang Reach (LJR) (Xia *et al.* 2016) (Figure 1(b)).

The Shashi Reach is located in the middle Yangtze River at approximately 194 km from the TGD, and it stretches approximately 74 km from Yangjianao to Yangchangzhen with an average channel width of 1,300–1,500 m. The whole Shashi Reach consists of four low-sinuosity bends, and each bend has a midchannel bar (Figure 1(c)). After completion of the TGD, the downstream channel evolution demonstrated evident temporal–spatial variations as a result of different inflow conditions and channel boundaries. As the first sandy-bed reach downstream, the Shashi Reach has a finer bed composition and thus undergoes more drastic morphological adjustments than the upstream sandy-gravel reaches. The channel evolution at the Shashi Reach is less affected by sediment supplementation than the reaches further downstream and has high susceptibility and dependence on upstream flow and sediment variations.

DATA COLLECTION AND METHODS

The flow and sediment conditions of the Shashi Reach were determined at the Shashi gauging station, which is situated approximately 208 km downstream of the TGD (Figure 1(c)). The related hydrological data covering the daily mean discharge and suspended sediment concentration at the Shashi station since 1992 and topographic maps with a scale of 1:10,000 measured in 2014.02 and 2014.12 at the Shashi Reach were collected from the Changjiang Water Resources Commission (CWRC, http://www.cjh.com) to investigate the flow-sediment regime alterations after dam construction and channel adjustments during a post-dam hydrological process. All the original data mentioned above underwent rigorous verification and uncertainty analyses following government protocols (Dai & Liu 2013) and were ensured reliable by the quality control imposed by the surveying agencies.

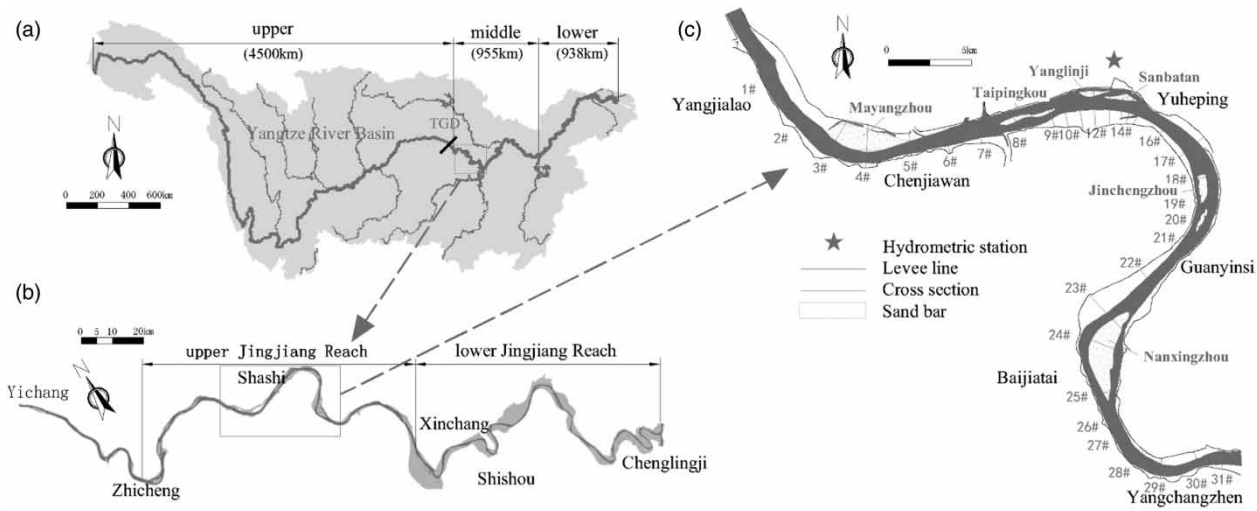

Figure 1 | Sketch maps of the (a) Yangtze River Basin, (b) Jingjiang Reach and (c) Shashi Reach with the Shashi gauging station location and cross-sections.

In the present work, we adopted a 2D hydro-morphodynamic model (details of model building and validation are included in the Supplementary Material, available with the online version of this paper) to investigate the responses of channel morphology to post-dam flow-sediment variations based on the 'real' hydrological process over 1 year. Because of the high peak discharge and representative flow regulation strategy, a hydrological process that occurred in 2014 at the Shashi Reach is used as the study case, which included the 2014 daily average discharge and sediment transport rate series observed at the Shashi station as the inputs for model validation and benchmark scenario. Then, we adopted a 'reconstruction' method to obtain another flow hydrograph that can reflect the natural flow regimes at the Shashi Reach and the impact of TGD flow regulation on the flow's seasonal distribution. This method is briefly explained as follows: assuming that the variation in the mainstream discharge of the Yangtze River caused by flow diversion and river confluence between the TGD and Shashi station can be viewed as invariant before and after dam construction, the preregulation (namely unregulated) flow discharge arriving at the Shashi Reach can be calculated simply as follows:

$$Q_{post} = Q_{pre} + Q_{in} - Q_{out} \tag{1}$$

where Q_{pre} and Q_{post} refer to the preregulation and post-regulation incoming flow discharge of the Shashi Reach, respectively, and Q_{in} and Q_{out} are the inflow and outflow discharges of the TGD, respectively. The daily average discharge data mentioned above can be downloaded from the official site of the China Yangtze Three Gorges Project Development Corp (CTGC, http://www.ctg.com.cn). Using this 'reconstruction' method, the preregulation flow hydrograph can be obtained (Figure 2). The preregulation flow discharges were notably reduced during the flood season (typically from May to October at the Jingjiang Reach (Xia *et al.* 2014)) and slightly augmented during the dry season, whereas the total water volume remained the same. To create flow hydrographs with similar temporal distribution characteristics but different peak discharges, the Gaussian function is applied to fit the field data and can be expressed as follows:

$$f(x) = y_0 + A/w\sqrt{\pi/2} \times \exp\{-2(x - x_c)^2/w^2\} \tag{2}$$

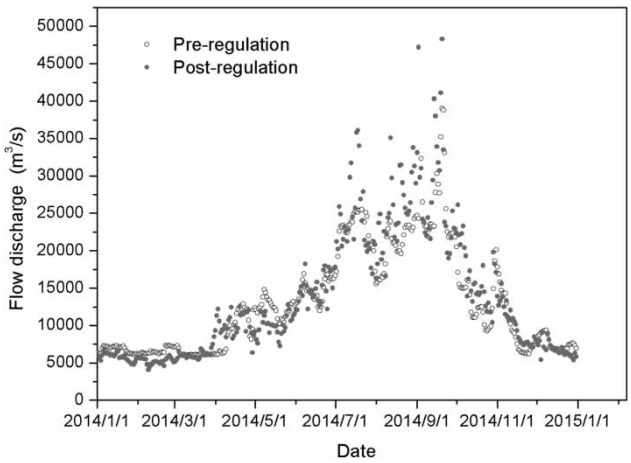

Figure 2 | 'Real' and 'reconstructed' hydrological processes in 2014 at the Shashi station.

where y_0, x_c, and A refer to the offset, centroid position, and covering area, respectively; and w is the width of the curve at the height of $(y_c - y_0)/2$. Three sets of value groups for these four parameters are attempted and determined, whereby three perfectly smooth hypothetical flow hydrographs can be obtained (Figure 3(a); we call these hydrographs F1 to F3 in the order of smallest to largest peak discharge) (Humphries *et al.* 2012; Guan *et al.* 2016).

Before matching the flow hydrographs with different sediment loads, we investigated the actual change in flow discharge-sediment transport rate relationships at the Shashi station. Using the observed flow-sediment data measured at the Shashi station, rating curves that reflect the sediment supply regimes can be fitted by a series of power functions (Figure 4) and the correlation coefficients of daily average flow discharge and sediment load are greater than 0.85 overall. As seen from Figure 4, even before the dam construction in 2003, the rating curves of the Shashi Reach from 1992 to 2002 displayed a declining trend due to the decrease in upstream sediment supply and river basin conservation measures (Yang *et al.* 2014). Immediately following the TGD completion in 2003, the rating curves dropped sharply, especially for large flow discharge, and the average sediment load during the post-dam period was nearly one order of magnitude less than that prior to dam construction. Given the construction of the Cascade Reservoirs in the upper Yangtze River, the sediment delivered into the Shashi Reach will be further reduced; thus a further decline in the rating curve will also

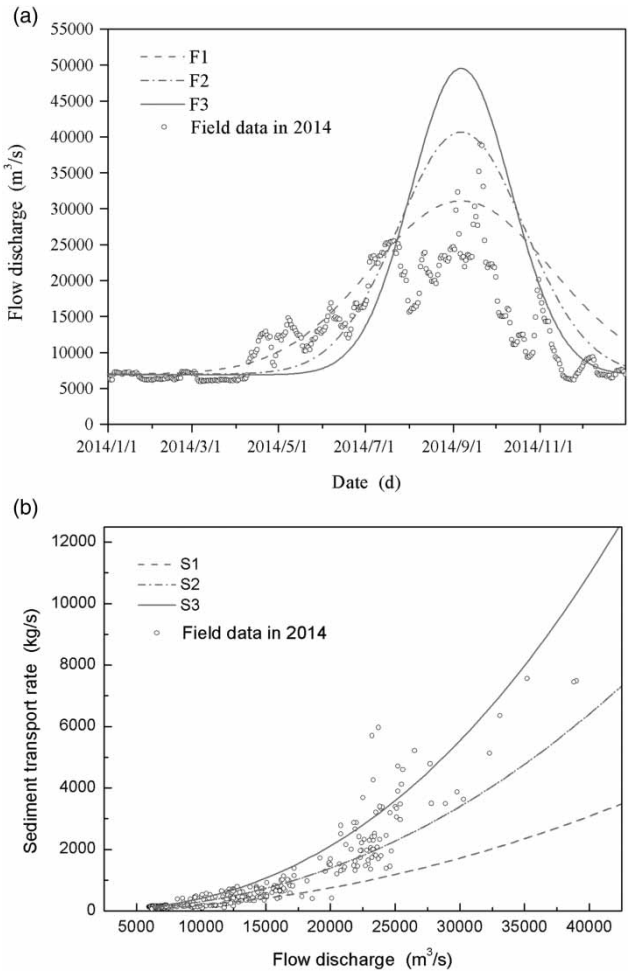

Figure 3 | Realistic process and three hypothetical hydrological processes (F1–F3) (a) and three hypothetical flow-sediment discharge rating curves (b).

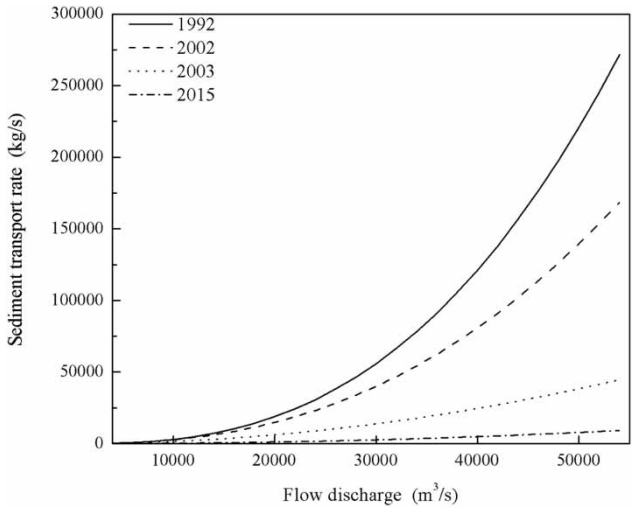

Figure 4 | Sediment rating curves before and after TGD construction.

be expected (Yang *et al.* 2014; Li *et al.* 2018a, 2018b). Based on this practical descending tendency, three rating curves after dam construction were selected, and they all vary obviously but are limited to a post-dam level (Figure 3(b); we call these curves S1 to S3 in the order of lowest to highest).

Thus far, all the input scenarios have been accomplished, and their designs are listed in Table 1. The annual flow and sediment runoff of these scenarios are listed in Table 2. As mentioned earlier, three flow hydrographs with different peak discharges are elaborated to hold the same total water volume to represent the effects of different flow regulation strategies, while three gradually decreasing rating curves are devised to reflect the sediment load reduction trend due to the construction of the Cascade Reservoirs in the upper Yangtze River. Therefore, the variations in post-run imprints caused by runs that have different flow hydrographs from F1 to F3 but with the same rating curve (S1 or S2 or S3) can be regarded as different flow hydrograph impacts. The variations in post-run imprints caused by runs that have different rating curves from S1 to S3 but with the same flow hydrograph (F1 or F2 or F3) can be regarded as different sediment supply regime impacts. Since this research mainly concerns morphological responses to different flow-sediment processes, the other inputs, including material composition and initial bed elevation, are kept identical for all runs.

RESULTS AND DISCUSSION

Morphological adjustments during the 2014 hydrological year

Although the 2014 hydrological process is not the focus of this present work, because it represents a 'real' post-dam scenario that occurred at the studied reach, the hydraulic and morphological changes produced by this scenario can provide details about the current river regime.

Figure 5 shows a plot of sediment volumes of net channel change as well as the gross erosion and deposition within the whole reach from a temporal perspective. The flow hydrograph is also included. The temporal change in gross erosion and deposition displayed high synchrony, which indicated that on the reach scale, riverbed erosion

Table 1 | Experimental scenario designs

Runs(R)	Flow hydrograph	Sediment supply regime	Purpose
R1	Virtual flow hydrograph with small peak F1	Lower rating curve S1	Quantification of channel's morphological response to different flow-sediment processes
R2	Virtual flow hydrograph with medium peak F1	Medium rating curve S2	
R3	Virtual flow hydrograph with large peak F1	Higher rating curve S3	
R4	Virtual flow hydrograph with small peak F2	Lower rating curve S1	
R5	Virtual flow hydrograph with medium peak F2	Medium rating curve S2	
R6	Virtual flow hydrograph with large peak F2	Higher rating curve S3	
R7	Virtual flow hydrograph with small peak F3	Lower rating curve S1	
R8	Virtual flow hydrograph with medium peak F3	Medium rating curve S2	
R9	Virtual flow hydrograph with large peak F3	Higher rating curve S3	
R10	'Real' flow hydrograph in 2014	'Real' rating curve in 2014	Model validation and morphological change investigation

Table 2 | Basic information on the flow and sediment inputs and corresponding channel changes

Conditions	Annual flow runoff (10^8 m^3)	Annual sediment runoff (10^4 t)	Annual net channel erosion (10^4 m^3)	Number of days during the flood season	Flow runoff during the flood season (10^8 m^3)	Sediment runoff during the flood season (10^4 t)	Net erosion during the flood season (10^4 m^3)
R1	5,246	2,095	903	183 (50.1%)	3,844 (73.3%)	1,845 (88.1%)	786 (87.3%)
R2	5,246	3,980	504	183 (50.1%)	3,844 (73.3%)	3,567 (89.6%)	437 (86.6%)
R3	5,246	6,243	97	183 (50.1%)	3,844 (73.3%)	5,678 (90.9%)	221 (68.1%)
R4	5,264	2,512	1,628	147 (40.3%)	3,742 (71.1%)	2,269 (90.3%)	1,470 (90.3%)
R5	5,264	4,960	1,029	147 (40.3%)	3,742 (71.1%)	4,567 (92.1%)	923 (89.7%)
R6	5,264	8,102	325	147 (40.3%)	3,742 (71.1%)	7,574 (93.5%)	247 (75.9%)
R7	5,252	2,910	2,131	125 (34.2%)	3,687 (70.2%)	2,679 (92.1%)	1,903 (89.3%)
R8	5,252	5,932	1,388	125 (34.2%)	3,687 (70.2%)	5,561 (93.7%)	1,194 (86.0%)
R9	5,252	10,008	459	125 (34.2%)	3,687 (70.2%)	9,517 (95.1%)	297 (64.7%)

Note: the percentage in bracket indicates the ratios of flood season values to annual total values.

is always accompanied by comparative deposition (Guan *et al.* 2016). However, the overall channel evolution was still dominated by net erosion and the high undersaturation degree of sediment laden flow favored more sediment entrainment in the flood or dry season (Li *et al.* 2018a, 2018b). Notably, the majority of the channel adjustments (77% for net erosion and 57% for gross erosion and deposition) occurred during the flood season (Ashraf *et al.* 2016), which indicated that larger floods during the flood season are the major cause of geomorphological changes in rivers despite their shorter duration than the frequent floods that occur during the dry season (Guan *et al.* 2016). According to the magnitude of the net erosion rate, the 1-year adjustment process could be divided into three intervals (see Figure 5), and they had daily average net erosion rates of 6,360 m^3, 32,726 m^3, and 14,765 m^3. After entering Interval II, the channel change rate sharply increased until reaching Interval III. Figure 11 shows that the critical discharge required to launch extensive sediment motion amounted to approximately 15,000 m^3/s, which was slightly less than the post-dam effective discharge calculated by Li *et al.* (2018a, 2018b).

As a key parameter in braided river research, the flow partition index is an important reference in the prediction of braided system evolution, maintenance of channel navigation conditions, and restoration of river ecological systems

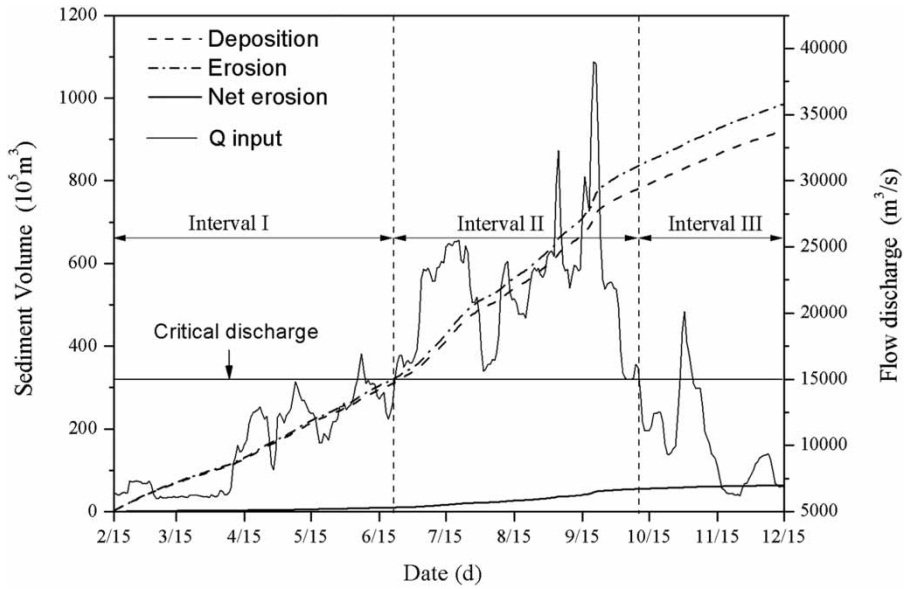

Figure 5 | Temporal variations in channel changes.

(Miori *et al.* 2012; Chalov & Alexeevsky 2015). The main branch location and its flow ratios at Taipingkou, Sanbatan, and Jingchengzhou before and after TGD construction are listed in Table 3 (due to a lack of data, Mayangzhou and Nanxingzhou are not included). Evidently, after TGD construction, an overall increase in the main branch flow partitions was discovered at Taipingkou and Sanbatan, while the main branch flow partition at Jinchengzhou was slightly decreased after TGD construction. The above changes in the flow distribution at each braided subsection can be rightly reflected in the results of our simulated initial-final riverbed. Since more silting-up occurred in the tributary branches, the main branch channels absorbed more flow discharge from the upstream, which induced more severe erosion within the deeper troughs (Chalov & Alexeevsky 2015). This phenomenon of tributary branch shrinkage and main channel incision is universal in post-dam channel evolutions of the middle and lower Yangtze River (Yang *et al.* 2014; Wang *et al.* 2016).

Table 3 | Low-flow partition index variations in the tributary branch before and after TGD completion based on field data

Measuring date	Flow discharge (m^3/s)	Taipingkou (%) *Right branch*	Sanbatan (%) *Right branch*	Jinchengzhou (%) *Left branch*
2001.2	4,370	32	57	97
2002.1	4,560	41	65	94
2003.3	3,728	45	73	–
2004.1	4,842	48	68	–
2005.11	8,703	55	55	87
2007.3	4,955	53	54	–
2009.3	6,907	62	57	90
2010.3	6,000	65	59	–
2011.2	5,933	61	40	–
2012.2	6,233	67	32	89
2013.2	6,130	58	39	–
2014.2	6,200	58	64	83
2014.12	7,000	*61*	*83*	*79*

Note: – indicates field data deficiency. The bold italic characters indicate main branch locations. The numbers in italics are the numerical simulation results.

Variations in net erosion volume during different flow-sediment processes

To investigate the morphological responses of the same initial channel to different flow-sediment processes, scenarios R1–R10 were implemented (Table 2). The temporal variations in net channel change are plotted in Figure 6. Intuitively, larger flood discharge and less sediment supply can intensify the net erosion (Dai & Lu 2010; Yang *et al.*

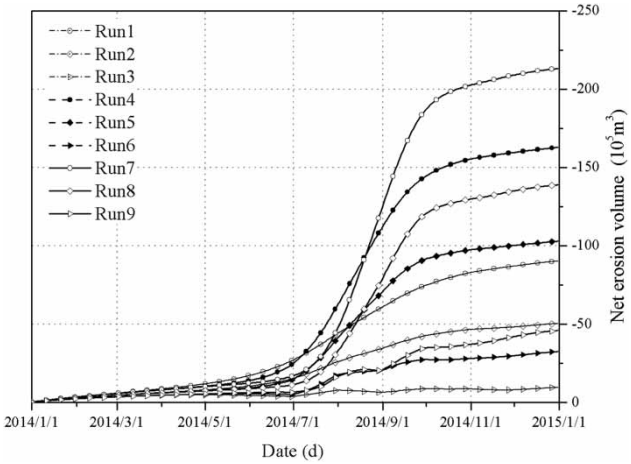

Figure 6 | Temporal evolution of the cumulative net changes during different runs.

2011). From a temporal view, we find that the channel adjustments during the flood season are the key for determining the resultant river morphology. Similarly, we take 15,000 m^3/s here as the critical discharge beyond which the motion of the bed surface sediment intensifies and the morphological significance of floods becomes apparent. Thus, for this study, the time when the daily average discharge exceeds 15,000 m^3/s can be counted as the flood season, and the corresponding flow and sediment statistics are listed in Table 2. In all runs, the ratios of flow runoff in the flood season to the total annual runoff are approximately the same (70%), and for the sediment load, these ratios are all greater than 88%, which generated 65%–90% of the net channel erosion according to different incoming water and sediment combinations. When the sediment delivery from the upstream decreases, the undersaturation degree of the sediment laden flow and the proportion of the net erosion during the flood season increased (Yang *et al.* 2014).

The current channel morphology at the Shashi Reach is undoubtedly the result of altered flow processes and sediment deficiencies caused by the TGD. However, regardless of the changes occurring in the inflow conditions, the imbalance between flow and sediment flux would ultimately be presented. To quantify this imbalance, some indicators composed of flow discharge and sediment concentration have been proposed in the Jingjiang research (Han 2015; Xia *et al.* 2016). In a similar way, we aim to find a comprehensive flow-sediment combination coefficient that is best correlated with the overall channel changes. First, we adopted the nonhomogeneous expression F proposed by Xia *et al.* (2016), which can be written as follows:

$$F = \frac{1}{N}\sum_{i=1}^{N}(Q_i^m/S_i)/10^{4m} \tag{3}$$

where Q_i and S_i are the daily average discharge (m^3/s) and sediment concentration (kg/m^3), respectively; and N denotes the total number of days in the flood season, and m represents the relative strength of the floods-caused erosion to sediment overloading-caused deposition. In Xia's research, m is set as 2 to define the average fluvial erosion intensity during the flood season. However, in the present work, the value of m is to be determined based on our simulation results. Thus, we used different values of m from 1 to 10 and then calculated the F value in all runs. The linear fitting of the overall net channel erosion and this parameter reveals the existence of an optimal value of m (Figure 7), which most significantly reflects the relative importance of flow to sediment flux in affecting downstream channel adjustments.

Figure 7 shows that m values of 2–4 can ensure greater statistical goodness of fit, which reaches the largest value when m equals 3. This finding indicates that the term Q_i^3/S_i can be the most appropriate indicator of the current flow-sediment imbalance regime at the Shashi Reach. This goodness of fit by the numerical simulation results reinforces the knowledge that although the fluvial geomorphology is determined by the collective effects of flow and sediment variations, the flow discharge and process variations may exert more significant influences on the flow-sediment imbalance than the changes caused by sediment supply regimes and result in more considerable channel morphological changes over the course of channel adjustments within the regulated river (Li *et al.* 2009).

Distribution of deposition and erosion

Since the subtle differences in 1-year geomorphological changes for all runs are difficult to clearly demonstrate using the plane distribution graph, we dissect the final river morphology by showing the channel changes that occurred at different channel elevations (Figure 8). Figure 8

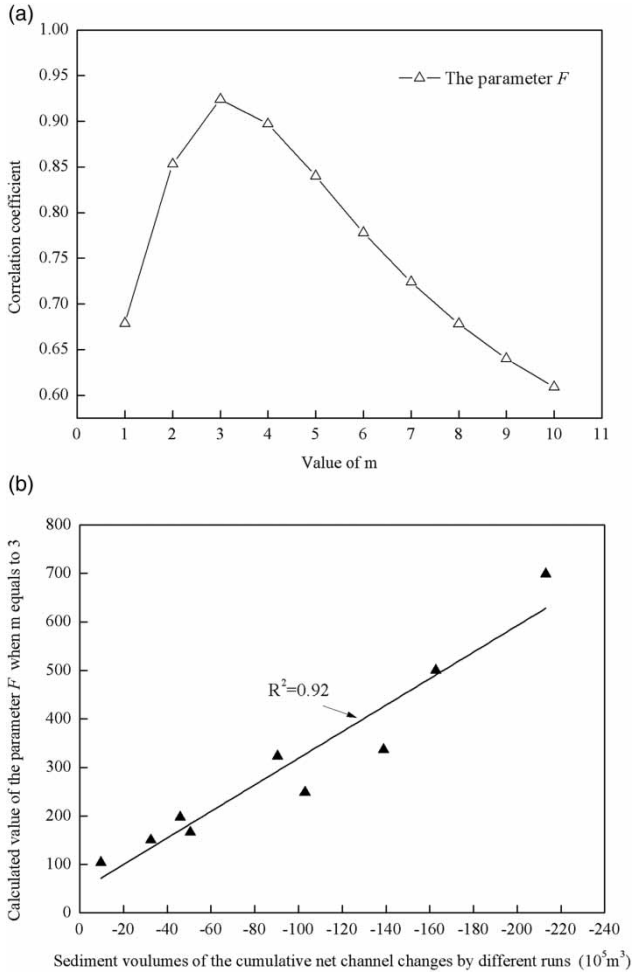

Figure 7 | Correlation coefficient between the exponent m of the parameter $F(=1/N)\sum_{i=1}^{N}(Q_i^m/S_i)/10^{4m}$) (a) and linear correlation between the optimum parameter F and the cumulative net channel change by different runs (b).

shows that sediment supply changes have greater effects on channels at lower elevations with the higher channels, which seldom have the chance to transport sediment, while the flow hydrograph changes can directly modify the scope where active flow and sediment exchanges occur, thus creating new areas of scoring and silting. As the magnitude of flood discharge increases, the channel scouring intensity is increased because of the greater stream power. The inundation area also expands due to a higher water stage, which enhances the flow momentum transfer between the main channel and floodplains (Wyżga *et al.* 2016). Compared with the change in flow conditions, the variations in sediment supply have little impact on the scope of where sediment can be transported to and usually play supplementary roles due to the great dependence between the sediment transport rate and hydrodynamics. Thus, we can expect that without processes such as riverbank collapse, river diversion, or tributary confluence, which can abruptly change the sediment concentration, the majority of shifts in deposition and erosion zones as well as the rearrangement of braiding systems mainly arise due to the occurrence of flood events and have little relationship with the change in sediment supply (Li *et al.* 2009; Staines & Carrivick 2015).

The regulated reaches in American rivers are reported to have more inactive flood plain areas than similar unregulated reaches due to the scarcity of less frequent flow discharges (Graf 2006). According to the measured data published by the CWRC, erosion downstream of the TGD is also reported to mainly occur in medium-flow channels (CWRC 2015). The channel change distribution presented above further corroborates, besides the erosion, that the deposition in the Shashi Reach also predominantly occurred within the medium-flow channel and was more difficult to extend to the higher part of the river corridor. To quantify the scouring-silting volumes that occur in different adjustment areas, the entire river channel is divided into low-flow, medium-flow, and bankfull channels corresponding to flow discharge rates of 5,000, 10,000, and 30,000 m^3/s, respectively, at the Yichang hydrologic station (CWRC 2015). By referring to the discharge hydrograph observed at Yichang station and the stage hydrograph observed at the Shashi station in 2014, we obtained the low-flow, medium-flow, and bankfull levels of the Shashi Reach, which were 26.604 m, 29.180 m, and 35.374 m, respectively. Therefore, the deposition and erosion within different channels under various conditions can be calculated, and the accumulation curves of channel deposition and erosion are plotted in Figure 9.

Consistent with the findings of the field data analysis (Zhang *et al.* 2016; Li *et al.* 2018a, 2018b), the outcomes of our mathematical simulation showed that most of the changes in channel erosion and deposition occurred in the medium-flow channel, which accounted for more than 70% of the total erosion and 77% of the total deposition in all runs (Figure 9). Above the bankfull level, few channel changes occurred in terms of erosion and deposition, which accounted for less than 9% and 8% of the total

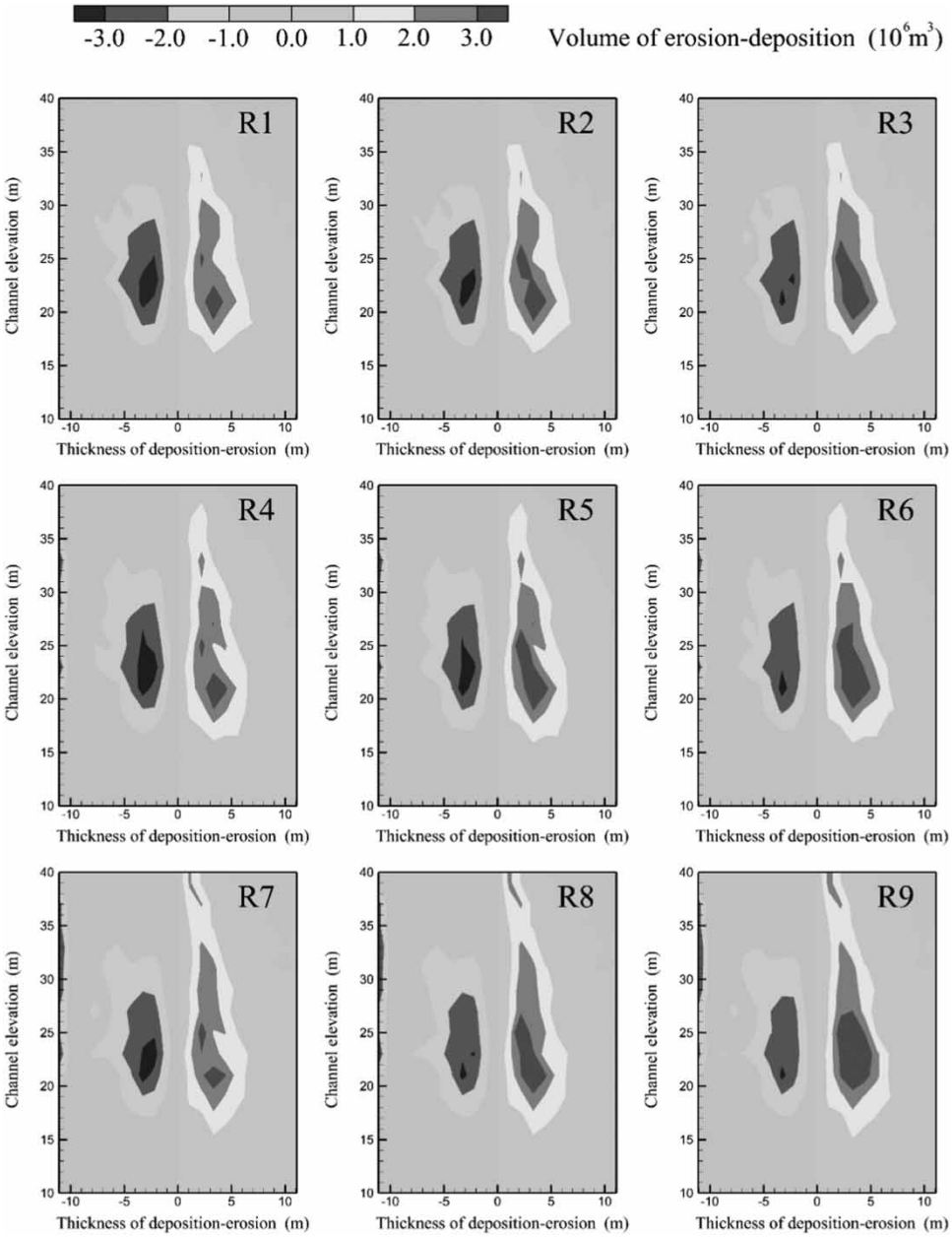

Figure 8 | Distribution of channel erosion and deposition amounts.

amounts in all runs, respectively. With larger flow discharges during the flood season, the erosion and deposition within all channels increased and the active areas of channel adjustment were extended to the higher parts of the channel corridors. Consequently, the proportions of erosion and deposition that occurred above the medium-flow channel both increased. However, the sediment supply variations mainly changed the deposition amount below the medium-flow channel, resulting in minute modifications in the channel adjustment area. With more sediment entering the studied reach, the erosion was lessened and deposition increased within all channels, with most predominantly occurring in the low-flow channel.

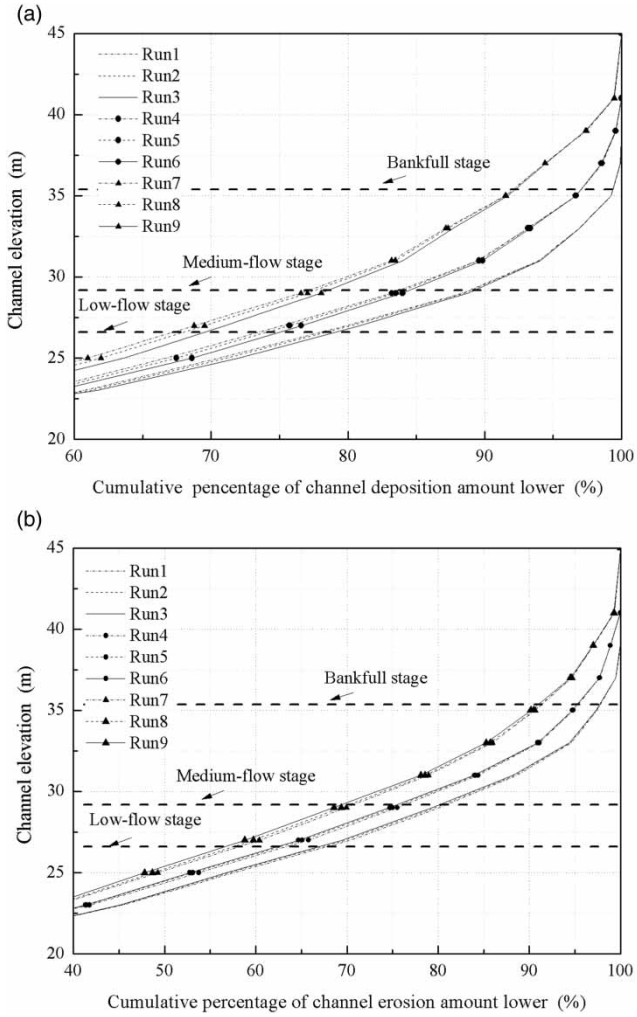

Figure 9 | Cumulative curves of channel deposition (a) and erosion (b).

Typical cross-section and riverbed thalweg profile variations

To further elaborate on the differences in channel morphological responses to various conditions, we examined the channel adjustments from the perspective of transverse and longitudinal changes. Because of the susceptibility of braided reaches to the inlet flow and sediment variations, the morphological behavior of branching channels and the attendant midchannel bars can strongly influence the evolution of the whole reach (Bolla Pittaluga *et al.* 2003; Bertoldi *et al.* 2010; Mueller & Pitlick 2014). Thus, four transverse sections crossing the braided reaches are taken as typical cross-sections to analyze the morphodynamic imprints of different runs (thereafter, we denote these imprints as T1–T9). In Figure 10, the branching sections showed no conforming deposition or erosion changes, and these sections were overall governed by a geomorphologic process that favored main branch development, namely less silting-up and more scouring within (Yang *et al.* 2014; Wang *et al.* 2016). Significant changes were not observed above the bankfull channel, and as the flow discharges increased during the flood season, both the erosion in the deeper channels and the deposition on the bar bodies were aggravated.

Figure 11 shows a plot of the thalweg profiles of the initial and shaped channels from different runs. For a clearer expression of the subtle differences, the original picture was truncated to the pieces that can reflect the major differences. Overall, the longitudinal thalweg displayed a declining tendency before or after the runs. Due to the inhomogeneous scouring of the low-flow channel, the post-run thalwegs exhibited more dramatic variations and larger fluctuation ranges, which were mostly ascribed to the channel incision caused by larger floods (Darby 2000; Wyżga *et al.* 2016). With larger flow discharge during the flood season, the lower sink of the thalwegs further decreased. With smaller flow discharges during the flood season, the higher bulges increased the most. These geomorphologic effects were conveyed downstream as the floods advanced, and the thalweg differences caused by different flow hydrographs could be seen from the reach inlet to outlet. However, variations in the impact of different sediment supplies were detectable only within a short distance from the inlet of the studied reach, which indicated a gradual unloading process of the overloaded sediment. Naturally, river channels can be aggradational due to sediment overloading (Millar 2005; Mueller & Pitlick 2014), and a sudden surge of sediment load in the flood season that far exceeded the sediment transport capacity is very likely to cause a decline in the overloaded sediment from the reach inlet (Pryor *et al.* 2011). Conversely, when the upstream inflow sediment load is abruptly reduced by natural events or human activities such as construction of the TGD, the proximal reaches downstream undergo the earliest channel degradation (Yang *et al.* 2011). These downstream-propagating disturbances are most commonly identified in dammed rivers, where channel degradation or aggradation immediately downstream of dams is gradually

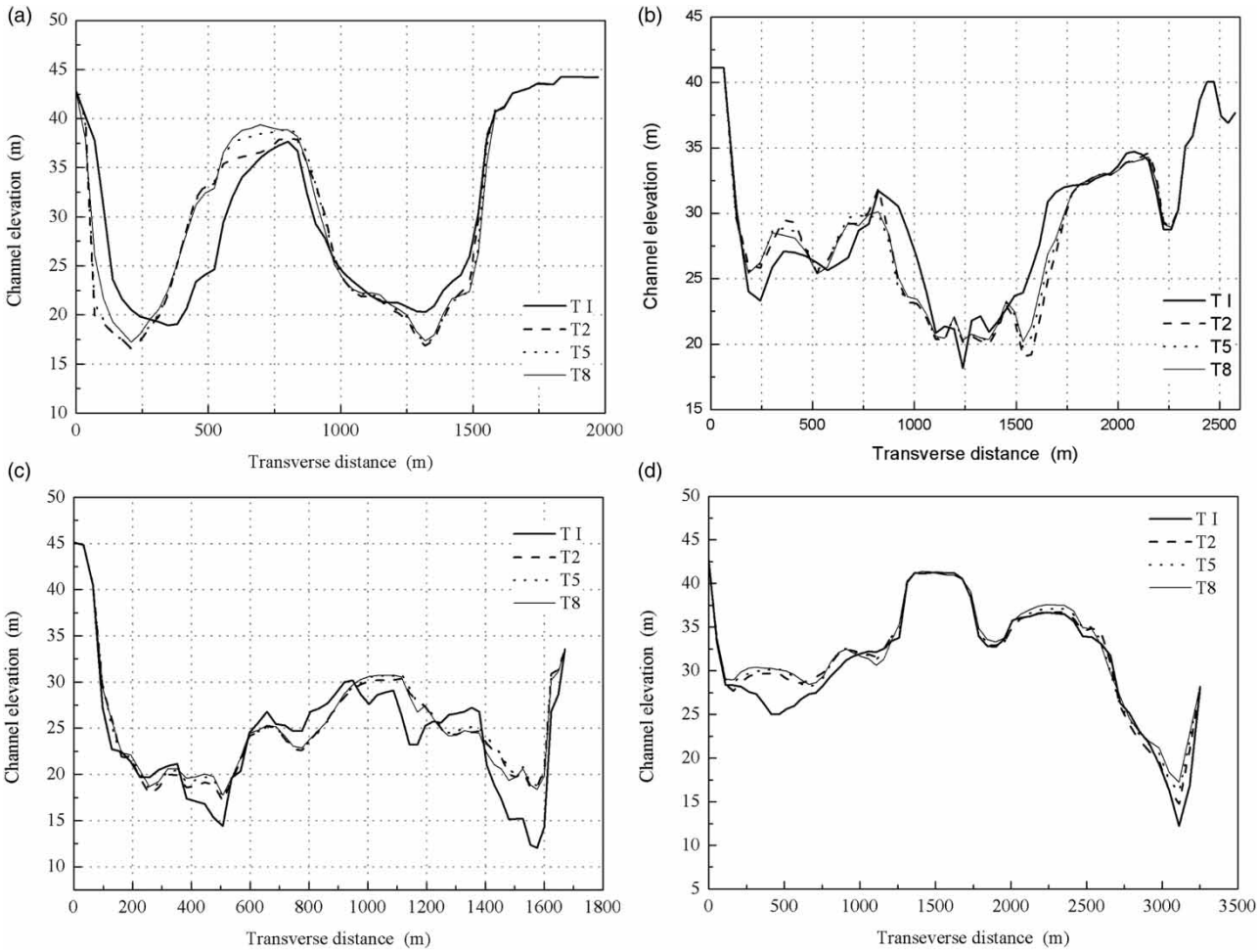

Figure 10 | Morphological changes in the typical cross-sections at Taipingkou (a), Sanbatan (b), Jinchengzhou (c), and Nanxingzhou (d).

mitigated by sediment replenishment or deficits along the river (Navratil *et al.* 2010; Heitmuller 2014).

Variations in channel geometry

Empirical relationships have been demonstrated between flow-sediment conditions and channel geometry, which commonly covers the channel width, channel depth, and cross-section area (Shin & Julien 2010; Shibata & Ito 2014). Based on post-dam field data at the reach downstream of the TGD, Zhou *et al.* (2017) developed high-correlation-degree quantitative relations between the reach-scale bankfull dimensions and the previous 5-year average fluvial erosion intensity. In this work, we first used the 2D hydrodynamic model to calculate the flow field distribution of the final channels shaped by the nine runs and then obtained the cross-section channel dimensions in low-flow, medium-flow, and bankfull channels. Then, an integrated method (Xia *et al.* 2014) was employed to calculate the reach average of the low-flow, medium-flow, and bankfull channel dimensions. By first calculating the corresponding cross-section values (the locations of the predetermined typical cross-sections are displayed in Figure 1(c)), the reach-average values can be written as follows:

$$\overline{G}_k = \exp\left(\sum_{i=1}^{N-1}(\ln G_k^{i+1} + \ln G_k^i) \times (x_{i+1} - x_i)/2L\right), \quad k = 1,3 \tag{4}$$

where $\overline{G}_k = (\overline{G}_{lf}, \overline{G}_{mf}, \overline{G}_{bf})$ represents the calculated reach-scale values in low-flow, middle-flow, and bankfull channels, which could be the channel width $\overline{W}_k$, the channel depth

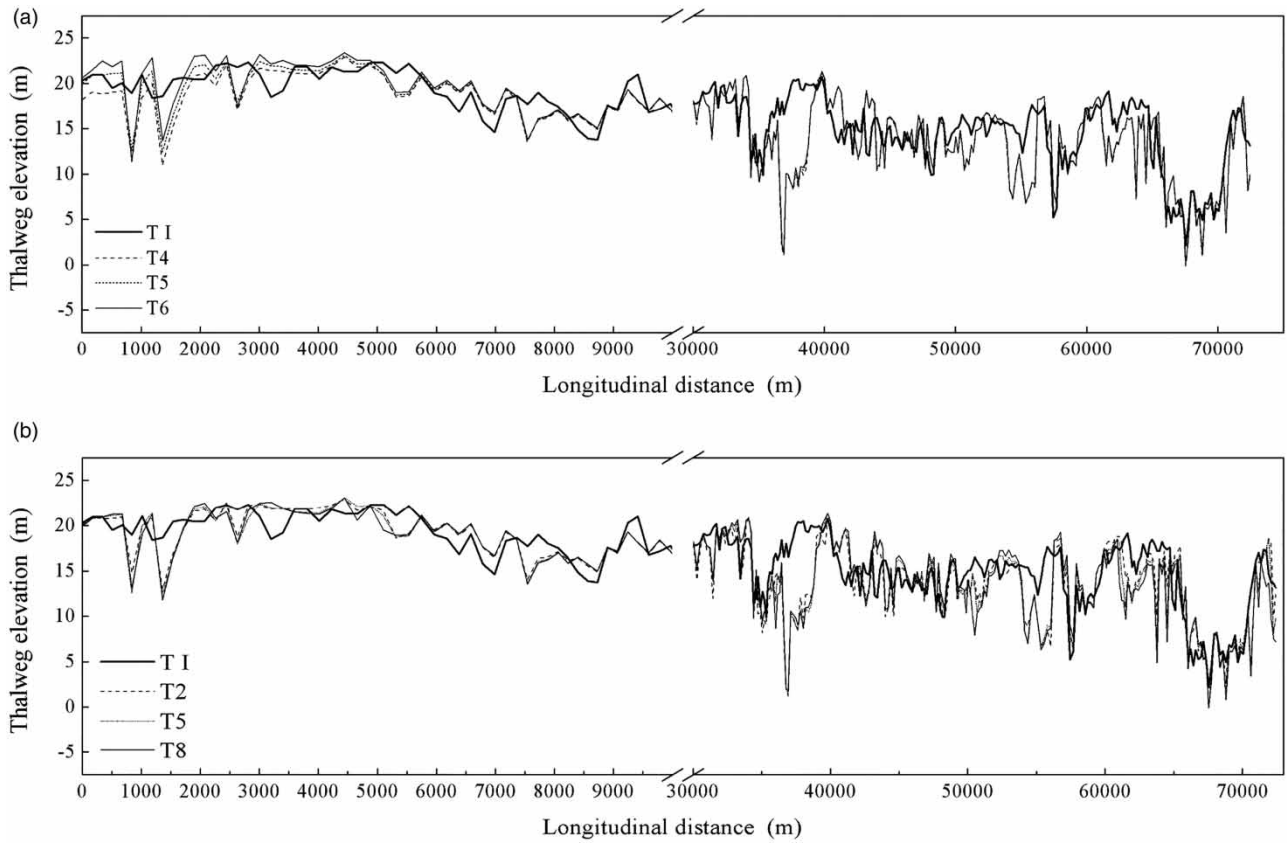

Figure 11 | Thalweg profile differences caused by variations in the sediment supply regime (a) and flow process (b).

$\overline{H}_k$, and the cross-section area $\overline{A}_k$; G_k^i and x_i represent the corresponding cross-section values and the longitudinal distance at the ith section, respectively; N is the number of selected cross-sections, with $N = 31$ the Shashi Reach and L the total reach length.

Figure 12 shows the results of the reach-scale channel width, depth, and cross-section area as well as the width-depth ratio of T1 to T9. Clearly, the post-run channels generally had greater channel depths and cross-section areas than the initial channel regardless of whether the channels were calculated in terms of low-flow, medium-flow, or bankfull channels. The largest percentage increases in the depth of the low-flow, medium-flow, and bankfull channels were 2.19, 2.97, and 2.26, respectively, and for the cross-section area, these values were 4.29, 2.30, and 0.98, respectively. However, with respect to the channel width, which directly influences the width-depth ratio, the variations showed different growing trends when calculated in terms of different channels. The post-run low-flow channel width became wider and presented a maximum increasing percentage of 2.44, whereas the medium-flow and bankfull width became narrower and presented maximum decreasing percentages of 0.81 and 1.48, respectively. Accordingly, the width-depth ratio increased in the low-flow channel and decreased in the medium-flow and bankfull channels. Therefore, the results indicate that during the typical post-dam hydrological process, the channel adjustments in the Shashi Reach were mainly characterized by an increase in channel depth and cross-section area (Zhang *et al.* 2016). The deep troughs below the low-flow level were further cut down and broadened, whereas above the low-flow level, the channel shrank with a slightly narrowing channel width (Graf 2006; Smith *et al.* 2016).

We also find that except for the channel width, the variations in channel depth, cross-section area, and width-depth ratio all showed consistent tendencies within the different channels. For example, with the increase in flood discharges from F1 to F3, the low-flow, medium-flow, and bankfull

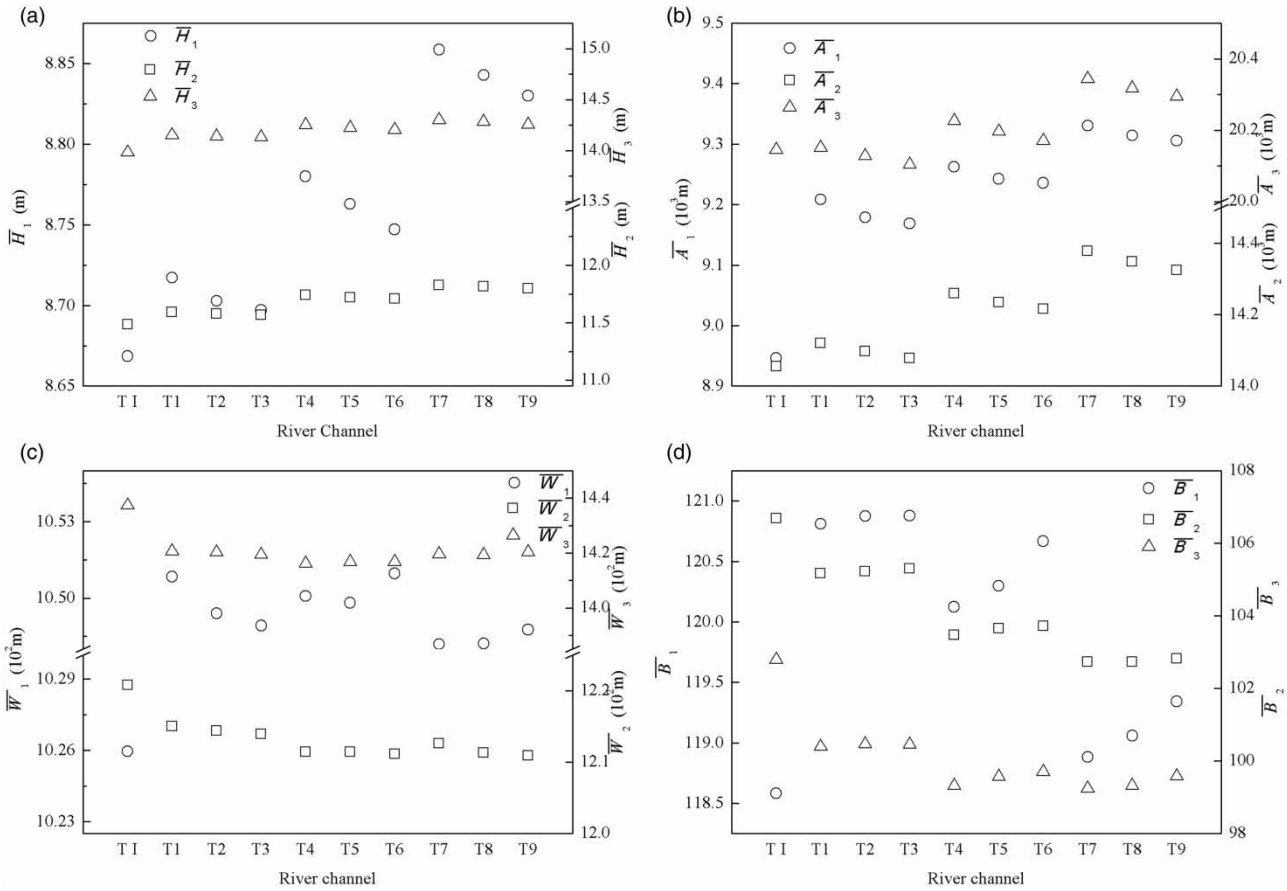

Figure 12 | Comparison of the reach-scale channel depth (a), cross-section area (b), channel width (c), and width-depth ratio (d) of the resulting channels shaped by different runs.

channel depths increased on average by 1.6%, 2.0%, and 1.0%, respectively, the cross-section area increased on average by 1.4%, 1.8%, and 0.9%, respectively, and the width-depth ratio decreased on average by 1.5%, 2.3%, and 1.1%, respectively. For the channel width, the calculated results demonstrated no consistent tendencies within the different channels, and even in terms of the same channel, the changes in channel width were inconsistent with that of flow or sediment flux. Bank erosion can be very intense for both sand-bed or gravel-bed large braided rivers (Takagi *et al.* 2007; Surian *et al.* 2009; Sarker *et al.* 2014). However, due to the effects of a series of river regulation works, the lateral deformation downstream of the TGD was somewhat limited and the variations in the reach-scale channel usually took a long time to detect (Zhou *et al.* 2017). Thus, the abnormal channel width variations obtained based on our simulation results can be partly attributed to the occurrence of bank revetment and shoal protection works at the Shashi Reach as well as the short simulation time.

CONCLUSIONS

Using a 2D hydro-morphodynamic model, the morphodynamic processes during different hypothetical flow-sediment processes were explored in this research, and these processes were constructed based on a 'real' hydrological event. Particular emphasis was placed on the discrepancies in channel morphological adjustments based on variations in the flow hydrograph and sediment supply regime. By examining the morphological changes during a 'real' hydrological process, we demonstrated that the post-dam channel adjustments in the Shashi Reach were dominated by net erosion and mainly characterized by an increase in channel depth and cross-sectional area.

The temporal variations in the net sediment volume change revealed that net channel erosion mainly occurred during the flood season, and even in the run that caused the largest amount of sediment deposition, the net erosion during the flood season accounted for approximately 65% of the total for the whole year. The higher flow hydrograph during the flood season and less sediment supply could lead to more drastic net erosion. Furthermore, we have quantified how different flow-sediment combinations can impact net channel changes. A high correlation was observed between the net erosion amount and the comprehensive flow-sediment combination coefficient $F = ((1/N)\sum_{i=1}^{N}(Q_i^3/S_i)/10^{12})$ at the Shashi Reach, which highlights the leading roles of flow hydrograph variations in downstream channel morphological adjustments in regulated rivers.

To further investigate the differences in channel morphological adjustment, we carefully compared the distributions of channel deposition and erosion. Longitudinally, the geomorphic effects of the flow hydrograph variations could be clearly observed along the whole reach, while the geomorphic effects of the sediment supply variations could be perceived only at a very short distance from the inlet of the studied reach. Vertically, the flow hydrograph variations could lead to changes in the inundation extent and even a shift in the active channel adjustment area, while the sediment supply regime variations had no impact on water stage and had little influence on the shift in the channel adjustment area. Therefore, the observed transfer of the adjustment area from the bankfull channel to the medium-flow channel at the Shashi Reach was more a consequence of the accumulated effects of the flow hydrograph variations than sediment supply changes.

These distribution discrepancies in channel deposition and erosion can eventually be expressed in the post-run channel geometries. Larger peak discharge during the flood season and less sediment supply could induce enlargements in the cross-sectional area, increases in channel depth, and decreases in the width-depth ratio. The largest percentage increases in the depths of the low-flow, medium-flow, and bankfull channels after runs were 2.19, 2.97, and 2.26, respectively, and for the cross-section area, these values were 4.29, 2.30, and 0.98, respectively. No consistent tendency was determined from the channel width results, which can be attributed to the occurrence of various river regulation works and the short simulation time.

ACKNOWLEDGEMENTS

This work was supported by the National Key Research and Development Program of China (Grant No. 2016YFC0402101) and the National Natural Science Foundation of China (Grant No. 51479146). We would like to thank the Yangtze River Water Resources Commission for providing important field data. The instructive suggestions by the editors and anonymous reviewers are gratefully acknowledged.

REFERENCES

Andrews, E. D. 1986 Downstream effects of Flaming Gorge Reservoir on the Green River, Colorado and Utah. *Geological Society of America Bulletin* **97**, 1012–1023.

Ashraf, M., Bhatti, M. T. & Shakir, A. S. 2016 River bank erosion and channel evolution in sand-bed braided reach of River Chenab: role of floods during different flow regimes. *Arabian Journal of Geosciences* **9**, 1–10.

Bertoldi, W., Zanoni, L. & Tubino, M. 2010 Assessment of morphological changes induced by flow and flood pulses in a gravel bed braided river: the Tagliamento River (Italy). *Geomorphology* **114**, 348–360.

Biedenharn, D. S., Thorne, C. R. & Watson, C. C. 2000 Recent morphological evolution of the Lower Mississippi River. *Geomorphology* **34**, 227–249.

Bolla Pittaluga, M., Repetto, R. & Tubino, M. 2003 Channel bifurcation in braided rivers: equilibrium configurations and stability. *Water Resources Research* **39**, 002283–002286.

Chalov, S. R. & Alexeevsky, N. I. 2015 Braided rivers: structure, types and hydrological effects. *Hydrology Research* **46**, 258–275.

Changjiang Water Resources Commission (CWRC) 2015 *Changjiang Sediment Bulletin*. Available from: http//www.cjh.com.cn (in Chinese).

Chen, J., Finlayon, B. L., Wei, T., Sun, Q., Webber, M., Li, M. & Chen, Z. 2016 Changes in monthly flows in the Yangtze River, China – with special reference to the Three Gorges Dam. *Journal of Hydrology* **536**, 293–301.

Dai, S. B. & Lu, X. X. 2010 Sediment deposition and erosion during the extreme flood events in the middle and lower reaches of the Yangtze River. *Quaternary International* **226**, 4–11.

Dai, Z. & Liu, J. T. 2013 Impacts of large dams on downstream fluvial sedimentation: an example of the Three Gorges Dam

(TGD) on the Changjiang (Yangtze River). *Journal of Hydrology* **480**, 10–18.

Darby, S. E. 2000 Incised river channels: processes, forms, engineering and management. *Geomorphology* **33**, 121–125.

David, M., Labenne, A., Carozza, J. & Valette, P. 2016 Evolutionary trajectory of channel planforms in the middle Garonne River (Toulouse, SW France) over a 130-year period: contribution of mixed multiple factor analysis (MFAmix). *Geomorphology* **258**, 21–39.

Graf, W. L. 2006 Downstream hydrologic and geomorphic effects of large dams on American rivers. *Geomorphology* **79**, 336–360.

Guan, M., Carrivick, J. L., Wright, N. G., Sleigh, P. A. & Staines, K. E. H. 2016 Quantifying the combined effects of multiple extreme floods on river channel geometry and on flood hazards. *Journal of Hydrology* **538**, 256–268.

Han, J. Q. 2015 *The Interaction Mechanism Between Longitudinal Water and Sediment Transport and Channel Morphology in the Downstream of Three Gorges Reservoir* (in Chinese). PhD Thesis, Wuhan University, Wuhan, China.

Heitmuller, F. T. 2014 Channel adjustments to historical disturbances along the lower Brazos and Sabine Rivers, south-central USA. *Geomorphology* **204**, 382–398.

Humphries, R., Venditti, J. G., Sklar, L. S. & Wooster, J. K. 2012 Experimental evidence for the effect of hydrographs on sediment pulse dynamics in gravel-bedded rivers. *Water Resources Research* **48**, W01533.

Legleiter, C. J. 2014 Downstream effects of recent reservoir development on the morphodynamics of a meandering channel: Savery Creek, Wyoming, USA. *River Research and Applications* **31**, 1328–1343.

Lenzi, M. A., Mao, L. & Comiti, F. 2006 Effective discharge for sediment transport in a mountain river: computational approaches and geomorphic effectiveness. *Journal of Hydrology* **326**, 257–276.

Li, Y., Sun, Z., Liu, Y. & Deng, J. 2009 Channel degradation downstream from the Three Gorges Project and its impacts on flood level. *Journal of Hydraulic Engineering* **135**, 718–728.

Li, D., Lu, X. X., Yang, X., Chen, L. & Lin, L. 2018a Sediment load responses to climate variation and cascade reservoirs in the Yangtze River: a case study of the Jinsha River. *Geomorphology* **322**, 41–52.

Li, S., Li, Y., Yuan, J., Zhang, W., Chai, Y. & Ren, J. 2018b The impacts of the Three Gorges Dam upon dynamic adjustment mode alterations in the Jingjiang reach of the Yangtze River, China. *Geomorphology* **318**, 230–239.

Ma, Y., Huang, H. Q., Xu, J., Brierley, G. J. & Yao, Z. 2010 Variability of effective discharge for suspended sediment transport in a large semi-arid river basin. *Journal of Hydrology* **388**, 357–369.

Millar, R. G. 2005 Theoretical regime equations for mobile gravel-bed rivers with stable banks. *Geomorphology* **64**, 207–220.

Miori, S., Hardy, R. J. & Lane, S. N. 2012 Topographic forcing of flow partition and flow structures at river bifurcations. *Earth Surface Processes and Landforms* **37**, 666–679.

Mueller, E. R. & Pitlick, J. 2014 Sediment supply and channel morphology in mountain river systems: 2. Single thread to braided transitions. *Journal of Geophysical Research: Earth Surface* **119**, 1516–1541.

Navratil, O., Legout, C., Gateuille, D., Esteves, M. & Liebault, F. 2010 Assessment of intermediate fine sediment storage in a braided river reach (southern French Prealps). *Hydrological Processes* **24**, 1318–1332.

Pal, S. 2016 Impact of Massanjore Dam on hydro-geomorphological modification of Mayurakshi River, Eastern India. *Environment, Development and Sustainability* **18**, 921–944.

Pryor, B. S., Lisle, T., Montoya, D. S. & Hilton, S. 2011 Transport and storage of bed material in a gravel-bed channel during episodes of aggradation and degradation: a field and flume study. *Earth Surface Processes and Landforms* **36**, 2028–2041.

Rădoane, M., Obreja, F., Cristea, I. & Mihailă, D. 2013 Changes in the channel-bed level of the eastern Carpathian rivers: climatic vs. human control over the last 50 years. *Geomorphology* **193**, 91–111.

Rickenmann, D., Badoux, A. & Hunzinger, L. 2016 Significance of sediment transport processes during piedmont floods: the 2005 flood events in Switzerland. *Earth Surface Processes and Landforms* **41**, 224–230.

Sarker, M. H., Thorne, C. R., Aktar, M. N. & Ferdous, M. R. 2014 Morpho-dynamics of the Brahmaputra-Jamuna River, Bangladesh. *Geomorphology* **215**, 45–59.

Scorpio, V. & Rosskopf, C. M. 2016 Channel adjustments in a Mediterranean river over the last 150 years in the context of anthropic and natural controls. *Geomorphology* **275**, 90–104.

Segura-Beltrán, F. & Sanchis-Ibor, C. 2013 Assessment of channel changes in a Mediterranean ephemeral stream since the early twentieth century. The Rambla de Cervera, eastern Spain. *Geomorphology* **201**, 199–214.

Shibata, K. & Ito, M. 2014 Relationships of bankfull channel width and discharge parameters for modern fluvial systems in the Japanese Islands. *Geomorphology* **214**, 97–113.

Shields Jr., F. D., Simon, A. & Steffen, L. J. 2000 Reservoir effects on downstream river channel migration. *Environmental Conservation* **27**, 54–66.

Shin, Y. H. & Julien, P. Y. 2010 Changes in hydraulic geometry of the Hwang River below the Hapcheon Re-regulation Dam, South Korea. *International Journal of River Basin Management* **8**, 139–150.

Smith, N. D., Morozova, G. S., Pérez-Arlucea, M. & Gibling, M. R. 2016 Dam-induced and natural channel changes in the Saskatchewan River below the E.B. Campbell Dam, Canada. *Geomorphology* **269**, 186–202.

Staines, K. E. H. & Carrivick, J. L. 2015 Geomorphological impact and morphodynamic effects on flow conveyance of the 1999 jökulhlaup at Sólheimajökull, Iceland. *Earth Surface Processes and Landforms* **40**, 1401–1416.

Surian, N. & Rinaldi, M. 2003 Morphological response to river engineering and management in alluvial channels in Italy. *Geomorphology* **50**, 307–326.

Surian, N., Mao, L., Giacomin, M. & Ziliani, L. 2009 Morphological effects of different channel-forming discharges in a gravel-bed river. *Earth Surface Processes and Landforms* **34**, 1093–1107.

Takagi, T., Oguchi, T., Matsumoto, J., Grossman, M. J., Sarker, M. H. & Martin, M. A. 2007 Channel braiding and stability of the Brahmaputra River, Bangladesh, since 1967: GIS and remote sensing analyses. *Geomorphology* **85**, 294–305.

Topping, D. J., Rubin, D. M. & Vierra, L. E. 2000 Colorado River sediment transport: 1. Natural sediment supply limitation and the influence of Glen Canyon Dam. *Water Resources Research* **36**, 515–542.

Tukur, A. L. & Mubi, A. M. 2002 Impact of Kiri dam on the lower reaches of river Gongola, Nigeria. *GeoJournal* **56**, 93–96.

Wang, J., Sheng, Y., Gleason, C. J. & Wada, Y. 2013 Downstream Yangtze River levels impacted by Three Gorges Dam. *Environmental Research Letters* **8**, 044012.

Wang, Y., Rhoads, B. L. & Wang, D. 2016 Assessment of the flow regime alterations in the middle reach of the Yangtze River associated with dam construction: potential ecological implications. *Hydrological Processes* **30**, 3949–3966.

Welber, M., Bertoldi, W. & Tubino, M. 2012 The response of braided planform configuration to flow variations, bed reworking and vegetation: the case of the Tagliamento River, Italy. *Earth Surface Processes and Landforms* **37**, 572–582.

Wyżga, B., Zawiejska, J. & Radecki-Pawlik, A. 2016 Impact of channel incision on the hydraulics of flood flows: examples from Polish Carpathian rivers. *Geomorphology* **272**, 10–20.

Xia, J., Zong, Q., Deng, S., Xu, Q. & Lu, J. 2014 Seasonal variations in composite riverbank stability in the Lower Jingjiang Reach, China. *Journal of Hydrology* **519**, 3664–3673.

Xia, J., Deng, S., Lu, J., Xu, Q., Zong, Q. & Tan, G. 2016 Dynamic channel adjustments in the Jingjiang Reach of the middle Yangtze River. *Scientific Reports* **6**, 22802.

Xu, J. 1996 Channel pattern change downstream from a reservoir: an example of wandering braided rivers. *Geomorphology* **15**, 147–158.

Xu, K. & Milliman, J. D. 2009 Seasonal variations of sediment discharge from the Yangtze River before and after impoundment of the Three Gorges Dam. *Geomorphology* **104**, 276–283.

Yang, S. L., Zhang, J. & Xu, X. J. 2007 Influence of the Three Gorges Dam on downstream delivery of sediment and its environmental implications, Yangtze River. *Geophysical Research Letters* **34**, L10401.

Yang, S. L., Milliman, J. D., Li, P. & Xu, K. 2011 50,000 dams later: erosion of the Yangtze River and its delta. *Global and Planetary Change* **75**, 14–20.

Yang, S. L., Milliman, J. D., Xu, K. H., Deng, B., Zhang, X. Y. & Luo, X. X. 2014 Downstream sedimentary and geomorphic impacts of the Three Gorges Dam on the Yangtze River. *Earth-Science Reviews* **138**, 469–486.

Yuill, B. T., Gaweesh, A., Allison, M. A. & Meselhe, E. A. 2016 Morphodynamic evolution of a lower Mississippi River channel bar after sand mining. *Earth Surface Processes and Landforms* **41**, 526–542.

Zahar, Y., Ghorbel, A. & Albergel, J. 2008 Impacts of large dams on downstream flow conditions of rivers: aggradation and reduction of the Medjerda channel capacity downstream of the Sidi Salem dam (Tunisia). *Journal of Hydrology* **351**, 318–330.

Zhang, W., Yuan, J., Han, J., Huang, C. & Li, M. 2016 Impact of the Three Gorges Dam on sediment deposition and erosion in the middle Yangtze River: a case study of the Shashi Reach. *Hydrology Research* **47**, 175–186.

Zhou, M., Xia, J., Lu, J., Deng, S. & Lin, F. 2017 Morphological adjustments in a meandering reach of the middle Yangtze River caused by severe human activities. *Geomorphology* **285**, 325–332.

First received 8 May 2019; accepted in revised form 18 July 2019. Available online 3 September 2019